Aminoacylation Reaction in the Histidyl-tRNA Synthetase: Fidelity Mechanism of the Activation Step

S. Dutta Banik and N. Nandi*

Department of Chemistry, University of Kalyani, Kalyani, Nadia, West Bengal, 741235, India

Received: November 11, 2009; Revised Manuscript Received: December 22, 2009

Aminoacylation is a vital step of natural biosynthesis of peptide. Correct aminoacylation is a necessary prerequisite for the elimination of noncognate amino acids such as D-amino acids. In the present work, we studied the fidelity mechanism of histidine (His) activation (first step of aminoacylation reaction) using a combined quantum mechanical/semiempirical method based on a model of crystal structure of the oligomeric complex of histidyl-tRNA synthetase (HisRS) from *Escherichia coli*. The study of the variation in the energy during the mutual approach of the His and ATP to form adenylate shows that the surrounding nanospace of synthetase confines the reactants (L-His and ATP) and proximally places in a geometry suitable for the in-line nucleophilic attack. The significantly higher energy of the energy surface of the model containing D-His is due to unfavorable interaction of D-His with ATP and surrounding residues. This indicates that the network of interaction (principally electrostatic) is highly unfavorable when D-amino acid is incorporated. The reorganization of the surrounding nanospace can lower the unfavorable nature of the intermolecular energy surface of D-His and surrounding residues. However, such a rearrangement requires large-scale structural reorganization of the synthetase structure and is unfavorable. The variation in the bond angles and distances in going from the reactant state to the product state via transition state confirms the mechanism of nucleophilic attack and concomitant inversion of oxygen atoms around α-phosphorus (α-P). Calculation of the electrostatic potential indicates that in addition to the Mg^{2+} the Arg residues in the active site facilitate the nucleophilic attack by reducing the negative charge distributed over the oxygen atoms attached to the α-P of ATP. Arg 259 residue has a role similar to that played by the two Mg^{2+} cations as this residue is in close proximity of the α-P of ATP. Arg 113 also facilitates the reduction of the negative charge on the other side of the reaction center. The favorable electrostatic interaction of the Arg 259 with ATP and His is also concluded from the calculation of the binding energy. The Arg 259 anchors the carboxylic acid group of His and the oxygen atom of the α-phosphate group during the progress of reaction. Consequently, Arg 259 plays an important catalytic role in the activation step rather than merely reducing the negative charge density over the ATP.

I. Introduction

Protein biosynthesis is a vital reaction which involves a number of macromolecules. The reaction takes place in successive stages like activation of amino acid followed by initiation, elongation, termination, release, folding, and post-translational processing.[1] The activation step for the aminoacylation reaction is an important biological reaction as it is the necessary prerequisite for the peptide bond formation. This step correlates the realm of the protein with the RNA world. The reaction involves adenosine triphosphate (ATP) and Mg^{2+} ion dependent aminoacyl tRNA synthetase (aaRS) to form aminoacyl adenylate followed by attachment of the amino acid to the tRNA. The aaRS specifically incorporates a particular amino acid and ensures that only cognate substrate is selected from the large cellular pool of similar amino acids. The specificity of the aaRS to incorporate a specific amino acid and its ability to discriminate between several competing substrates is well-known.[2] The frequency of misincorporation of noncognate amino acid is 1 in 10^4, which is a surprising accuracy.[3] This accuracy is one of the major requirements for the accurate translation of the genetic code.

The structural basis of amino acid and ATP recognition and the mechanism of activation are studied in detail for class I and class II synthetases from crystallographic studies, kinetic studies, and mutation experiments. An in-line displacement mechanism followed by the nucleophilic attack by the carboxyl group of the amino acid on the α-phosphate of the ATP is suggested for the first step of the aminoacylation reaction.[4,5] The role of various active site residues in the discrimination and fidelity mechanism is proposed based on crystallographic studies. An early proposition is that the editing and acylation site which are complementary pairs of sites function as a double filter.[3] It is suggested that the acylation site might reject amino acids larger than the correct one because there is insufficient space for them. On the other hand, the smaller amino acids are cleaved by the hydrolytic editing site. Notably, this size- or volume-based mechanism is not capable to discriminate the enantiomeric species of the cognate amino acid as the D- and L-enantiomers occupy identical total volume. However, a number of experimental studies unambiguously established that the process of aminoacylation is stringent about incorporation of the L-enantiomer.[6]

Experimental studies indicate that the specificity is present at the level sufficient to discriminate the enantiomeric species.[7−13] Neither the acylation site nor the editing site would be able to discriminate the enantiomers if the size factor is essentially

* Corresponding author. E-mail: nilashisnandi@yahoo.com. Fax: 91-33-25828282.

10.1021/jp910730s
Published on Web 01/27/2010

controlling the proofreading process. The discrimination by aaRS can be better understood in terms of the interactions (principally electrostatic) between the aaRS and the amino acid. This view is supported by recent computational studies on aminoacylation of the AspRS[14] and HisRs.[15] The preference for acylation of L-Asp over D-Asp and L-Asn by Aspartyl-tRNA synthetase (AspRS) is studied using molecular dynamics simulation.[14,16] The studies point out that the influence of the network of electrostatic interaction present in AspRS protects against most binding errors. Discrimination against D-Asp can be explained by unfavorable binding with the D-Asp. On the basis of component analysis, it is indicated that Coulomb interactions with the protein are the major favorable factor to the L-Asp binding. It is also concluded that the cobinding of ATP and its three divalent cations does not significantly affect binding specificity. Chiral discrimination is also studied for the first step of aminoacylation reaction by HisRS using combined *ab initio*/semiempirical calculation.[15a] The relative ease of the rotatory path for the approach of D-amino acid toward the ATP in the activation step is shown as different from that of the L-amino acid. Their nanoscale separation is also an important factor for the discrimination. The transition state structure is suggested to be different for the alteration of chirality which can contribute to the discrimination. The network of electrostatic interaction within the nanospace enclosed by the active site residues is perturbed when the D-amino acid is incorporated. The pathway to the transition state corresponding to the activation by D-His is also unfavorable due to the lack of stabilizing interactions in the transition state structure corresponding to the activation by L-His. However, the study is based on a simplified model which is necessary to be improved to incorporate the electrostatic interactions in detail.

Foregoing computational studies complement the view that a number of intricate contacts between aaRS and amino acid, which is favorable for cognate but unfavorable for noncognate amino acids, make the successful recognition and the concomitant discrimination. A specific molecular mechanism is expected to be involved for each synthetase to distinguish the correct pair of substrates from the pool of amino acids and tRNA molecules. There may be a succession of discriminating processes, but the molecular mechanism for the surprising accuracy and fidelity is yet to be understood. While the overall reaction mechanism of the activation is proposed from crystallographic structures[4,5] and simulations using classical force field,[16] the molecular mechanism of the fidelity of the activation step is yet to be understood in detail from first principles.[15a]

The mechanism of activation of His has been proposed based on detailed analysis of the crystal structure of *Thermus thermophilus* histidyl-tRNA synthetase.[5] An in-line displacement mechanism followed by the nucleophilic attack by the carboxyl group of the amino acid on the α-phosphate of the ATP leads to the formation of histidyl adenylate. It is proposed that Arg 259 might play a catalytic role in conservation and in close proximity with the reactants. It is also suggested that this residue along with Arg 112 neutralizes the negative charge over the carboxyl group of His and stabilizes the pentavalent transition state proposed based on the crystal structure analysis. However, the exact role played by Arg 259 and Mg^{2+} ions, although found necessary, was not unambiguously established. The mechanism of activation of His is also proposed by detailed analysis of the crystal structure of *Escherichia coli* histidyl-tRNA synthetase.[4] However, to the best of our knowledge, only limited detailed electronic structure based analysis has been carried out,[15a] and it is worthwhile to study the discrimination in a more detailed way.

In the present work, we have studied the fidelity mechanism for the preference of L-His over D-His (a chiral discrimination) by HisRS for the first step of the aminoacylation reaction using combined ab initio/semiempirical method. The detailed structure of the active site of HisRS is analyzed to identify the active site residues that might play a role in the fidelity mechanism.[4] We studied the electrostatic interaction in the potential energy surface of the reactant by identifying relevant variables corresponding to the process of the nucleophilc attack of His to ATP (within the active site) out of the complete coordinate manifold of the reaction pathway. The potential energy surface of the active site in the reactant state is complex as the reaction coordinate space is large for such biological systems. In general, such a complex system is expected to have a multitude of minima.[17] A comparison of the variation in interaction energies as a function of the identified variables for the incorporation of L-amino acid and D-amino acid is expected to reveal the fidelity mechanism. Such variables are inter- as well as intramolecular coordinates of reactant (His, ATP) and surrounding. These variables significantly change during the reaction. The study is also expected to reveal which active site residues might play a significant role in protecting the misincorporation of D-amino acid.

The transition state structure and the transition state barrier height could be different for alteration of chirality which can contribute to the chiral specificity in the activation step of aminoacylation. A preliminary study supports the foregoing view. This factor is also known to contribute in the chiral discrimination in the process of peptide bond formation in ribosomes.[6] In such complex systems, individual minima are clustered into "basins" separated by energy barriers, and internal distribution between basins is separated by a small-energy barrier.[18] Electronic structure based methods are useful in studying the corresponding potential energy surfaces, transition state barrier height, and stabilizing interactions of the transition state. A transition state can be identified by the frequency analysis[19] and can not be confirmed unambiguously based on the information about the thermodynamically average states as obtained from crystal structure analysis. The pentacovalent transition states proposed from crystallographic studies formed by nucleophilic attack on the tetracoordinated phosphorus atom have biological significance and have been analyzed by ab initio studies in other systems.[20] Hence, an electronic structure based analysis is expected to be useful in understanding the reaction mechanism in the aminoacylation reaction.

The details of the combined ONIOM ab initio/semiempirical calculation are described in section II. Results are presented and analyzed in section III, followed by concluding remarks.

II. Theoretical Calculation

The crystal structures of the oligomeric complex of histidyl-tRNA synthetase (HisRS) from *Escherichia coli* complexed with ATP and histidinol (an inhibitor) and histidyl-adenylate (PDB ID: 1KMM and 1KMN)[21] are used to generate the models of the active site of reactant and product. The $-CH_2OH$ group of the histidinol moiety is replaced by the carboxylic acid group to construct the His in the model of the active site. In addition to the His and ATP, the model of the active site also includes Glu-83, Arg-113, Gln-127, Glu-131, Arg-259, Tyr-264, Gly-304, Phy-305, and Ala-306 (all numbering corresponds to the scheme as in HisRS from *Escherichia coli*; PDB ID: 1KMN,

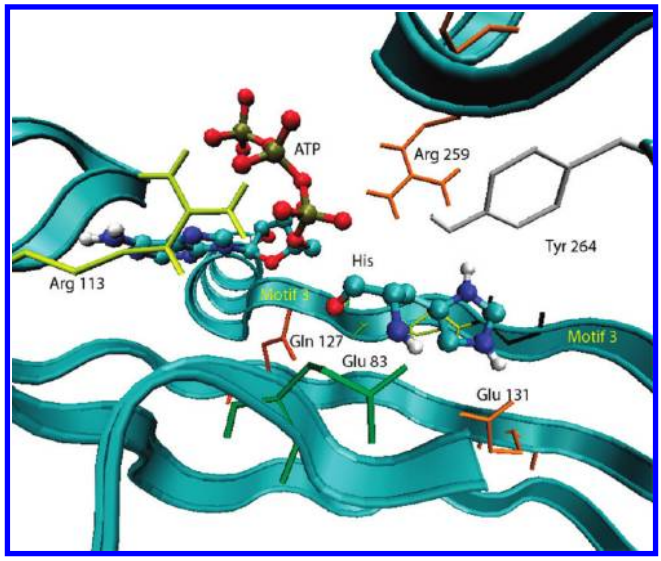

Figure 1. Active site of the crystal structure of the HisRS−Histidinol−ATP complex (PDB code: 1KMN).[21] The structure is the basis of the model used in the present work (details are described in section II). The reactants (histidinol and ATP) are shown in CPK style. Side chains of the active site in close proximity of the reactants as Glu 83, Arg 113, Gln 127, Glu 131, Arg 259, and Tyr 264 are shown by bonds. The remaining part of the motif 2, His A loop and motif 3, is represented by ribbons. For details, see text. The image is prepared using VMD.[28]

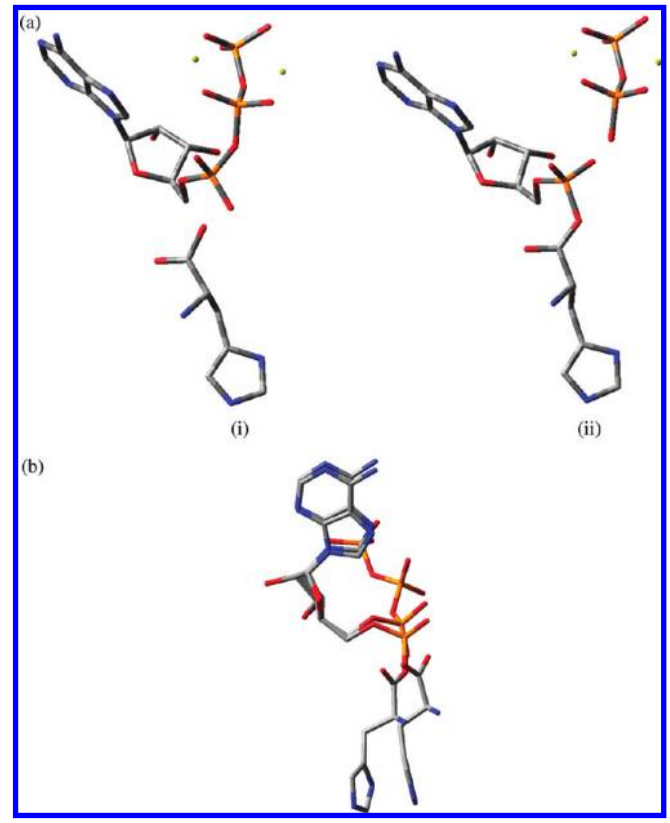

Figure 2. (a) Comparison of the (i) reactant and the (ii) product geometry based on the model of reactant and product ($Model_{Reactant(L)}$ and $Model_{Product(L)}$) as obtained from reactant and product crystal structure (PDB code: 1KMN and 1KMM, respectively).[21] For details, see section II. A change in the orientation of the amino acid moiety relative to the ATP occurs as shown in Figure a(i) and a(ii), respectively. (b) The overlay of reactant and product structures indicating the displacement of the imidazole group of the His moiety toward the plane containing the sugar ring of the ATP coupled with a change of the orientation of the carboxylic acid group of the His in going from the reactant state to the product state. The Cartesian coordinates are given in Table II(a) of the Supporting Information.

1KMM).[21] These residues are in close proximity of the reactants in the active site. The residues Arg-259 and Tyr-264 belong to the HisA loop. Tyr-264 is hydrogen bonded to the imidazole group of the His. Arg-113, Gln-127, and Glu-131 residues belong to motif 2. Arg-113 is a conserved residue in *E. coli*, *Streptococcus equis*, *Saccharomyces cerevisiae*, *Caenorhabditis elegans*, and *Homo sapiens* and might have a role in the progress of reaction.[4] Gln-127 is hydrogen bonded to the amino group of the His substrate. Glu-131 is in close proximity of the ε2 atom of His. Gly-304 is a conserved residue in *E. coli*, *Streptococcus equis*, *Saccharomyces cerevisiae*, *Caenorhabditis elegans*, and *Homo sapiens*.[4] Phe-305 and Ala-306 enclose the reactants in a nanospace to provide suitable positioning of the reactants. The carboxylic group of Glu-83 of helix AH3 forms a salt-bridge with the α-amino group of the His[21] and is included in the present model. The structure is shown in Figure 1. The model also includes two Mg^{2+} ions (indicated as Mg^{2+} 2 and Mg^{2+} 3)[22] located near the $\beta-\gamma$ phosphate linkage. This is shown in Figure S.1 of the Supporting Information. As mentioned before, the Arg 259 which is suggested to act as a substitute for one of the three Mg^{2+} ions (Mg^{2+} 1 near the α and β phosphate)[22] as present in all class II synthetases[21] is also included. One water molecule as observed in the crystal structure is included near the Mg^{2+} 2 as shown in Figure S.1 of the Supporting Information. The second water molecule is hydrogen bonded with the NH_3^+ group of His. These two water molecules are present in the crystal structure in close proximity of the His and ATP. The corresponding model of the reactant and product state is denoted by $Model_{Reactant}$ and $Model_{Product}$ respectively.

The model structure of the active site (total number of atoms is 170) is optimized using the two-level ONIOM (HF/6-31G**:PM3) method. The histidine and α and β phosphorus of ATP with attached oxygen and the sugar ring are considered at high level. Remaining atoms of the reactant and surrounding residues are considered at low level. The electrostatic potentials for reactants (His and ATP) as well as surrounding residues of the active site are computed using the HF/6-31G** level of theory using Mulliken population analysis. The D-His is generated in the active site by exchanging the proton and the amino group (as this exchange is least unfavorable). The generation of D-His by other possible exchanges of groups involving the side chain and the carboxylic acid group is highly unfavorable for the product state leading to the progress of reaction. The conformational energy difference between the L-His and D-His is only 1.34 kcal/mol at the HF/6-31G** level, and the results are independent of the conformational energy difference of the two enantiomers.

Comparison of the reactant and the product geometry shows that a change in the distance and orientation of the amino acid moiety relative to the ATP occurs in a plane containing the α-P atom of ATP, the carboxyl carbon of amino acid, and the chiral carbon of amino acid and is nearly perpendicular to the plane containing the imidazole ring of the histidine moiety as shown in Figures 2(a)(i) and 2(a)(ii), respectively. The following angle and dihedral angles are varied to study the structural changes involved related to the His and ATP in the reactant and product state. The overlay of reactant and product crystal structures (1KMN and 1KMM, respectively) as shown in Figure 2(b) indicates that the plane containing the imidazole group of the His moiety is displaced toward the plane containing the sugar ring of the ATP coupled with a change of the orientation of the carboxylic acid group of the His which

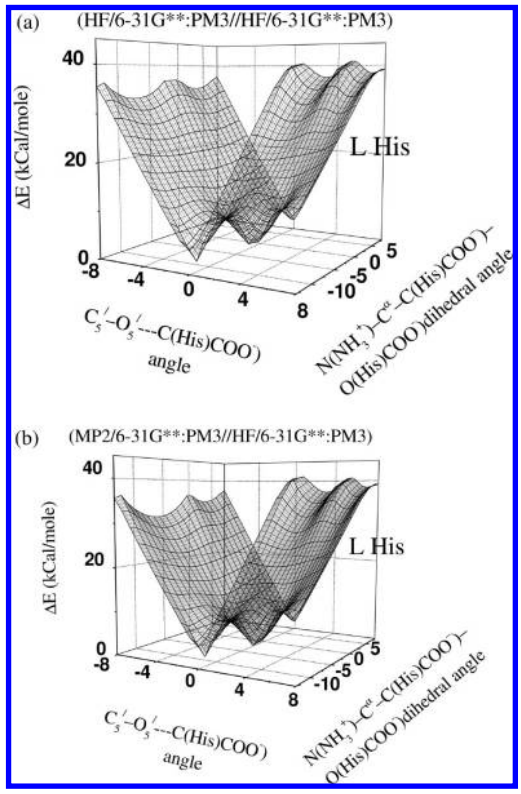

Figure 3. Variation of the interaction energy as a function of the orientation of the His moiety (expressed in degrees) and the orientation of the carboxylic acid group of His relative to the ATP (expressed in degrees) in the presence of active site surrounding residues as studied using optimized geometry, $Model^{Opt}_{Reactant\ (L)}$. The Cartesian coordinates are given in the Table II(b) of the Supporting Information. Starting from the $Model^{Opt}_{Reactant\ (L)}$ state, the His is orientated (expressed in degrees) in a plane containing the C5′−O5′···C(COO⁻His) atoms (nearly perpendicular to the plane containing the imidazole group of the His) as shown in Figure S.2 (Supporting Information). Simultaneously, the orientation (expressed in degrees) of the carboxylic acid group of His is varied with respect to the α NH_3^+ group of His. The variation in the energy is computed using (a) two-level ONIOM (HF/6-31G**:PM3//HF/6-31G**:PM3) and (b) the variation of the interaction energy as shown in (a) using a two-level ONIOM (MP2/6-31G**:PM3//HF/6-31G**:PM3) method.

aligns the O(COO⁻)−C(COO⁻)−O(COO⁻)···P(ATP) dihedral angle from its state in reactant to the product state. The energy variations related to the changes in the foregoing change in distance and orientation are studied by varying the C_5'(ATP)−O_5'(ATP)···C(^{His}COO⁻) angle and the N(His)−C^α−C(^{His}COO⁻)−O(^{His}COO⁻) dihedral angle. This pair of angle and dihedral angles (as shown in Figure S.2 of Supporting Information) can be used to investigate the relative ease of the changes in the distance and orientation between ATP and cognate (L-His) or noncognate amino acid which is necessary for the approach of the amino acid (cognate or noncognate) toward the ATP in going to the product state. The variation in the energy is computed by using two-level ONIOM (HF/6-31G:PM3//HF/6-31G:PM3) as well as by incorporating electron correlation using a two-level ONIOM (MP2/6-31G**:PM3//HF/6-31G**:PM3) method. His as well as α and β phosphorus of ATP with an attached oxygen and the sugar ring are considered at high level, and all the surrounding residues are considered at lower level. The results are shown in Figures 3(a,b) and Figure 4, respectively.

The changes in intra- and intermolecular variable of His and ATP occur within the confined state surrounded by a set of active site residues. These residues confine the amino acid and

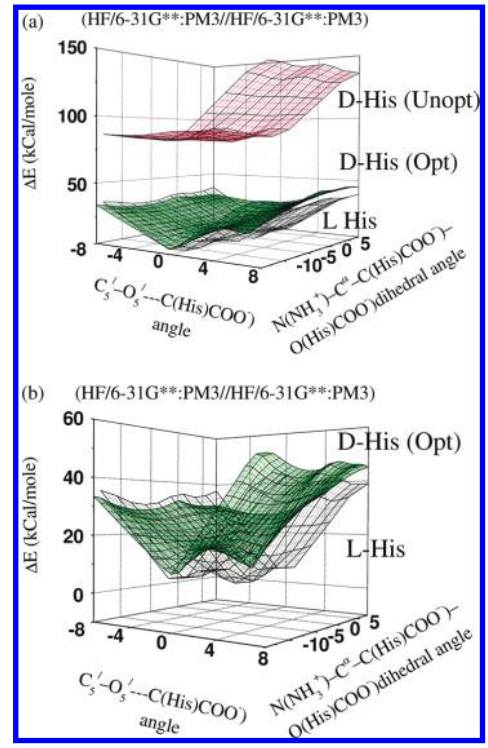

Figure 4. (a) Comparison of the variation of the interaction energy as a function of the orientation of the His moiety (expressed in degrees) and the orientation of the carboxylic acid group of His relative to the ATP (expressed in degrees) as shown in Figure 3 for $Model^{Opt}_{Reactant\ (L)}$, $Model^{Opt}_{Reactant\ (D)}$, and $Model^{Unopt}_{Reactant\ (D)}$. The Cartesian coordinates are given in Table II(b) of the Supporting Information. For details, see section II. The variation in the energy is computed using two-level ONIOM (HF/6-31G**:PM3//HF/6-31G**:PM3). (b) Comparison of the variation of the interaction energy as shown in (a) with the interaction energy difference between $Model^{Opt}_{Reactant\ (L)}$ and $Model^{Opt}_{Reactant\ (D)}$ in an enlarged scale.

ATP to carry over to the product state and create a network of electrostatic interaction. We studied the effect of individual residues on discrimination by varying the mutual distances between the respective residues and the reactants (His and ATP) which change during the reaction. The details of the variations in the mutual distances between Glu-83, Arg-113, Arg-259, and Tyr-264 residues and the His moiety and ATP are described in section A of the Supporting Information. Consequently, the study of the variations in the interaction energy as a function of these sets of variable is expected to be useful in understanding the stability of the cognate L-His in going through the reaction path in the active site and exclusion of noncognate D-His. The calculation of the interaction energies is performed using the two-level ONIOM (HF/6-31G**:PM3) method based on the $Model_{Reactant(L)}$ and $Model_{Reactant(D)}$. Two different theoretical levels of calculations are considered. In the first calculation, each of the active site residues (Glu-83, Arg-113, Arg-259, and Tyr-264) are considered at lower level (PM3), and these residues are incorporated at the HF level in the other set of calculations. The results are shown in Figures 5−8, respectively. We also carried out ONIOM (HF/3-21G*: PM3 level) calculation of the transition state geometry for the activation step. The structure for the reactant, transition state, and product is shown in Figures 9(a−c), respectively. The transition state is identified by a single imaginary frequency. The scheme of the reaction is shown in Figure 10.

We calculated the variation in the electrostatic potential during the course of the reaction for the reactant and the product state.

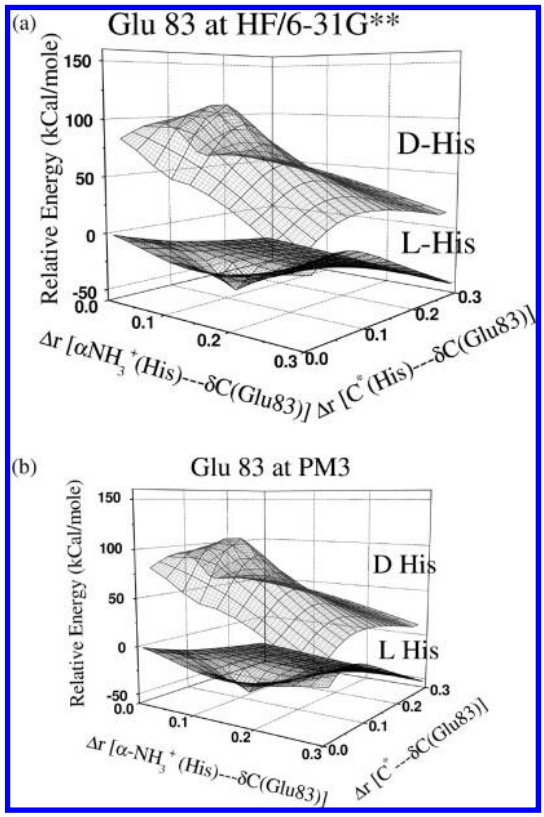

Figure 5. Variation in interaction energy as a function of relative distance between the nitrogen atom of the α-amino group of His and δC of Glu-83 (Å) as well as the relative distance between the chiral center of His and δC of Glu-83 (Å) for $Model_{Reactant(L)}$ and $Model_{Reactant(D)}$ with rigid geometry. Starting from the mutual arrangement of Histidine and Glu 83, as in the crystal structure mutual separation is varied as present in the product state $Model_{Product(L)}$. The Cartesian coordinates are given in the Table II(c) of the Supporting Information. Computations are performed using the two-level ONIOM (HF/6-31G**:PM3) method (a) variation in interaction energy as shown in (a) with Glu 83 at the HF/6-31G** and in (b) with Glu 83 considered at the PM3 level.

The electrostatic potential, $V(\vec{r})$ that the electrons and nuclei of a molecule create at each point $\vec{r}$ in the surrounding space is given by[23]

$$V(\vec{r}) = \sum_{A} \frac{Z_A}{|\vec{R}_A - \vec{r}|} - \int \frac{\rho(\vec{r}')d\vec{r}'}{|\vec{r}' - \vec{r}'|} \qquad (1)$$

Z_A is the charge of the nucleus A, located at $\vec{R}_A$. The electronic density function of the molecule is denoted by $\rho(\vec{r})$. The contour of the electrostatic potential (ESP) (calculated at the HF/3-21G* level of theory using an isodensity value of 0.0004 au) in a plane containing the carboxylic carbon atom, oxygen atom of His, and α-phosphorus atom of ATP is shown in Figures 11(a,b) for the optimized reactant and product state. To understand the role of the Arg 113 and Arg 259 in the reaction, we also analyzed the electrostatic potential surfaces of the reacting substrates in the geometry as present in the $Model_{Reactant(L)}$ calculated at the HF/6-31G** level of theory in the absence and presence of these residues (shown in Figures S.4 and S.5 of Supporting Information). We also computed the transition state barrier height of the reaction by altering the capacity of the Arg residue to form hydrogen bonds. The Gaussian 03 suite of programs was used.[24] Results are described in the following section.

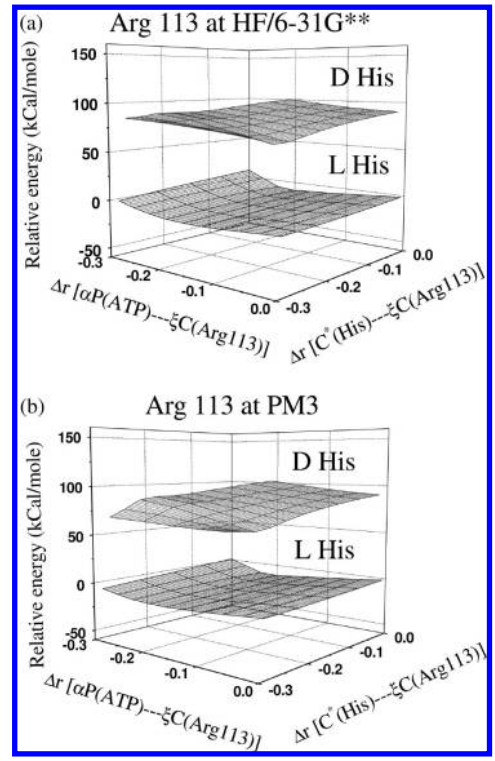

Figure 6. Variation in interaction energy as a function of relative distance between the α phosphorus atom of ATP and ξC of Arg-113 (Å) as well as the relative distance between the chiral center of His and ξC of Arg-113 (Å) for $Model_{Reactant(L)}$ and $Model_{Reactant(D)}$ with rigid geometry. Starting from the mutual arrangement of Histidine or ATP and Arg 113 as in the crystal structure, mutual separation is varied as present in the product state $Model_{Product(L)}$. The Cartesian coordinates are given in Table II(c) of the Supporting Information. Computations are performed using the two-level ONIOM (HF/6-31G**:PM3) method (a) with Arg 113 at the HF/6-31G** and (b) with Arg 113 considered at the PM3 level.

III. Results and Discussion

The variation in the energy during the mutual approach of the His and ATP to form adenylate is shown in Figure 3(a) based on two-level ONIOM calculation using the HF/6-31G**:PM3//HF/6-31G**:PM3 method. The plot expresses the change of the potential energy as a function of coordinates which are changing during the progress of the reaction with L-His (as discussed in section II). The energy surface has small barriers with a local and global minimum. The plot shows that the surrounding nanospace of synthetase confines the L-His and ATP in the global minima of the plot and proximally places the reactants in geometry suitable for the in-line nucleophilic attack. The incorporation of electron correlation using a two-level ONIOM (MP2/6-31G**:PM3//HF/6-31G**:PM3) does not change the nature of the potential energy surface as shown in Figure 3(b).

The corresponding variation in energy for D-His within the identical arrangement of the surrounding residues as present in the case of L-His is highly unfavorable as shown in Figure 4(a). The corresponding unoptimized geometry is denoted as $Model^{Unopt}_{Reactant(D)}$. The unfavorable nature of the energy surface of the $Model^{Unopt}_{Reactant(D)}$ relative to the model containing L-His is due to the loss of the favorable interaction between the surrounding residues of the active site and D-His compared to the L-His. Note that the difference in the conformational energies of the L- and D-His is not responsible for the rise in energy as observed in Figure 4(a) as the energies of the isolated L-His

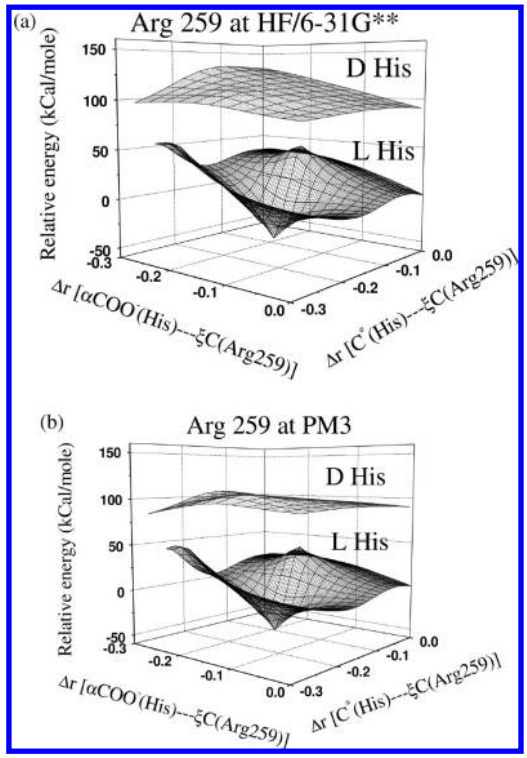

Figure 7. Variation in interaction energy as a function of relative distance between the carbon atom of the α carboxylic acid group of His and ξC of Arg-259 (Å) as well as the relative distance between the chiral center of His and ξC of Arg-259 (Å) for $Model_{Reactant(L)}$ and $Model_{Reactant(D)}$ with rigid geometry. Starting from the mutual arrangement of Histidine and Arg 259 as in the crystal structure, mutual separation is varied as present in the product state $Model_{Product(L)}$. The Cartesian coordinates are given in Table II(c) of the Supporting Information. Computations are performed using the two-level ONIOM (HF/6-31G**:PM3) method (a) with Arg 259 at the HF/6-31G** and (b) with Arg 259 considered at the PM3 level.

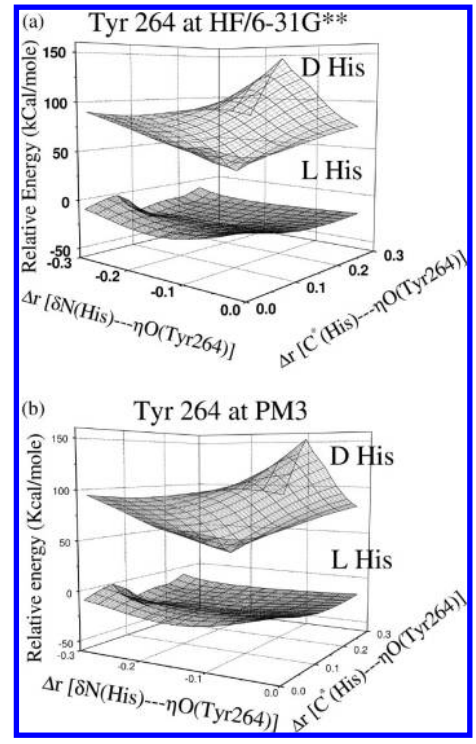

Figure 8. Variation in interaction energy as a function of relative distance between δN of His and ηO of Tyr-264 (Å) as well as the relative distance between the chiral center of His and ηO of Tyr-264 (Å) for $Model_{Reactant(L)}$ and $Model_{Reactant(D)}$ with rigid geometry. Starting from the mutual arrangement of Histidine and Tyr 264 as in the crystal structure, mutual separation is varied as present in the product state $Model_{Product(L)}$. The Cartesian coordinates are given in Table II(c) of the Supporting Information. Computations are performed using the two-level ONIOM (HF/6-31G**:PM3) method (a) with Tyr 264 at the HF/6-31G** and (b) with Tyr 264 considered at the PM3 level.

and D-His moieties in the respective models differ only by 1.34 kcal/mol at the HF/6-31G** level of theory. The result indicates that the discrimination of L-His and D-His is controlled by the active site nanospace. The significantly higher energy of the energy surface of the model containing D-His is due to unfavorable interaction of D-His with ATP and surrounding residues. It was noted earlier that the confinement of reacting moieties placed within the nanometer regime of an active site of a biological reaction can drive the corresponding reaction very precisely with remarkable discrimination capacity.[6] The present result shows that the same principle is also responsible for the discrimination between L-His and D-His in the activation step of the aminoacylation reaction.

The unfavorable nature of the potential energy surface of $Model^{Unopt}_{Reactant(D)}$ becomes substantially favorable (but still higher on an average by at least ~5 kcal/mol) when the structure is optimized and the surrounding residues are reorganized to lower the interaction energy between the residues and D-His (as shown in Figures 4(a) and 4(b), respectively). However, the active site residues in closest proximity of His have undergone significant reorganization in the $Model^{Opt}_{Reactant(D)}$ relative to the $Model^{Unopt}_{Reactant\ (D)}$ or $Model^{Unopt}_{Reactant\ (L)}$. Large-scale rearrangements of the peptide linkage of the respective motifs and helices occur during optimization. We have compared the model of active site with D-His in the optimized state (denoted as $Model^{Opt}_{Reactant(D)}$) with the corresponding optimized L-structure (denoted as $Model^{Opt}_{Reactant(L)}$). This is shown in Figure S.3(a−d) of the Supporting Information. In all cases, the reorganization is disruptive to the overall structure of the synthetase. Consequently, the incorporation of the D-His into the synthetase leading to a possible formation of D-Histidinyl adenylate is highly unfavorable. The foregoing result shows that the set of active site residues confines the amino acid and ATP in a potential well using orientation- and distance-dependent interaction which is selective of the natural L-His for adenylation.

The variations in the interaction energy as a function of intermolecular distances between His, ATP, and the respective surrounding residues such as Glu-83, Arg-113, Arg-259, and Tyr-264 and concomitant effect on discrimination is shown in Figures 5−8, respectively. The variations in energy reveal the relative stability of the cognate amino acid (L-His) compared to the D-His as a function of the separation between the surrounding residues and His.

The results of the variation of the potential energy as a function of variation of the relative distance between the nitrogen atom of the α-amino group of His and δC of Glu-83 and the chiral center of His and δC of Glu-83, calculated at the HF/6-31G**:PM3 level of theory (considering Glu 83 at the HF level and PM3 level, respectively), are shown in Figure 5(a) and Figure 5(b), respectively. The plot shows that the interaction energies of the L-His and D-His with Glu 83 are not identical with the variation of the distance between the nitrogen atom of the α-amino group of His and δC of Glu-83 (indicated as $\Delta r[\alpha\text{-}NH_3^+(His)\cdots\delta C(Glu83)]$) and with the variation of the relative distance between the chiral center of His and δC of Glu-83 (indicated as $\Delta r[C^*(His)\cdots\delta C(Glu83)]$). The result shows that the energy surface is more favorable with increasing $\Delta r[\alpha$-

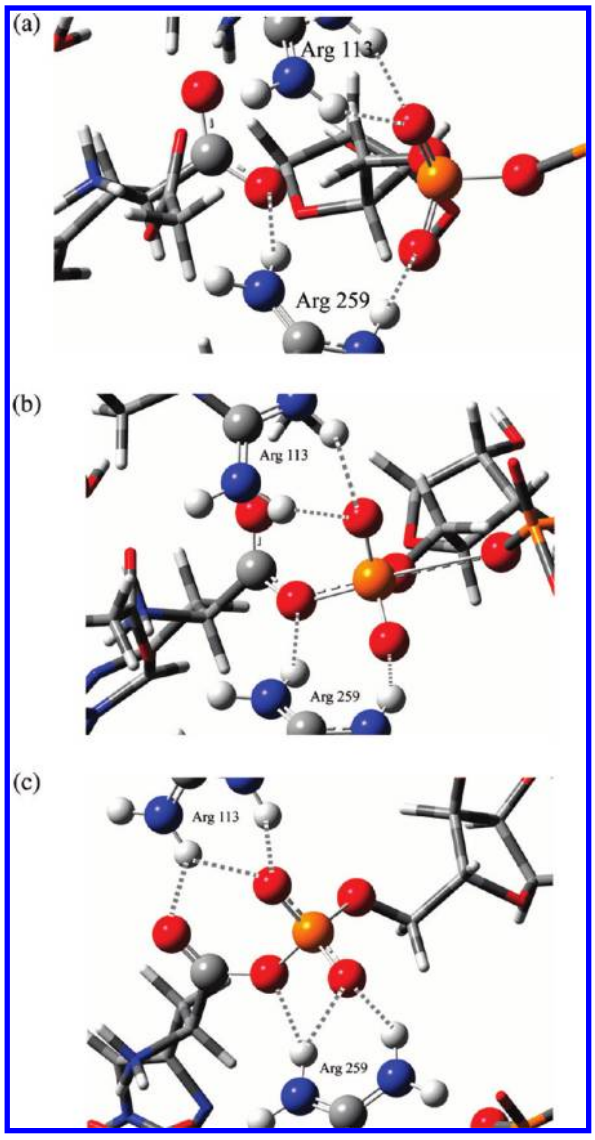

Figure 9. Optimized geometries of the (a) reactant, (b) transition state, and (c) product of the activation step of aminoacylation reaction using ONIOM (HF/3-21G*: PM3) level calculation. Side chains of the active site residues in close proximity of the reactants as Glu 83, Gln 127, Arg 113, and Arg 259 are included in the calculation. The details of the model are described in section II. The atoms participating in the reaction pathway are highlighted. The Cartesian coordinates are given in Table II(d) of the Supporting Information.

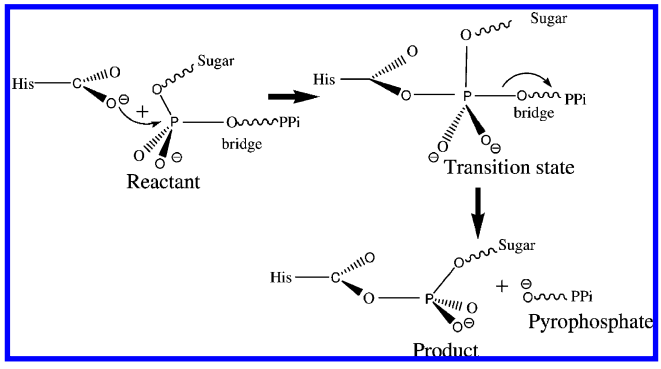

Figure 10. Schematic representation of the reactant, product, and transition state of the activation step of the aminoacylation reaction.

NH_3^+(His)···δC(Glu83)] (from reactant to product state). Also, the interaction energy of the L-His is passing through a minima, whereas that of the D-His is passing through a maxima. The

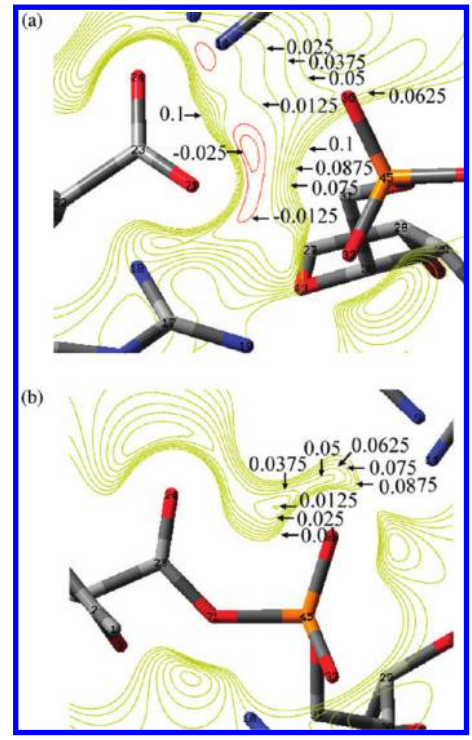

Figure 11. Contour plots of the electrostatic potential of the (a) optimized reactant and (b) optimized product of the activation step of aminoacylation reaction (corresponding to the optimized structures as shown in Figures 9(a) and (c), respectively) at the HF/3-21G* level of theory. The contours are drawn at intervals of 0.0125 au. The range of the electrostatic potential is considered as ±0.1 au.

difference in energy between $Model_{Reactant(L)}$ and $Model_{Reactant(D)}$ is due to the difference in the separation of the positively charged amino group of His and the negatively charged carboxylic acid group of Glu-83 in the respective cases. The unfavorable nature of the energy surface of the D-His indicates that the electrostatic interaction of Glu 83 with His protects against the activation by the wrong enantiomer. The features of the plots at the different level of theories considered (HF or PM3) are similar, indicating that the conclusions are independent of the theoretical method used.

The variations of the energy surface as a function of relative distances between the αP atom of ATP and ξC of Arg-113 (indicated as Δr[δP(ATP)···ξC(Arg113)]) and the chiral center of His and ξC of Arg-113 (indicated as Δr[C*(His)···ξC(Arg113)]) for the $Model_{Reactant(L)}$ as well as $Model_{Reactant(D)}$ calculated at the HF/6-31G:PM3 level of theory including Arg 113 at the HF level and PM3 level are shown in the Figures 6(a) and 6(b), respectively. The surface of $Model_{Reactant(D)}$ is higher in energy with respect to the energy surface of the $Model_{Reactant(L)}$. The energy surface for L-His has a minimum at reduced Δr[δP(ATP)···ξC(Arg113)] separation and is due to the favorable electrostatic interaction between ATP and Arg-113 at close separation. On the other hand, no minima are noted for $Model_{Reactant(D)}$, and the surface is unfavorable on an average.

Figures 7(a) and 7(b) show the variation of the potential energy as a function of variation of the relative distance between the carbon atom of the α carboxylic acid group of His and ξC of Arg-259 (indicated as Δr[αCOO$^-$(His)···ξC(Arg259)]) and the chiral center of His and ξC of Arg-259 (indicated as Δr[C*(His)···ξC(Arg259)]) for the $Model_{Reactant(L)}$ and $Model_{Reactant(D)}$ at the HF/6-31G **:PM3 level of theory including Arg 259 at the HF level and PM3 level, respectively. The result

shows that the energy surface of $Model_{Reactant(L)}$ has a distinct minimum which is absent in the $Model_{Reactant(D)}$ energy surface, and a barrier is noted in the later case as a function of the variation of the mutual separation between D-His and Arg 259. The energy is most favorable when the separation $\Delta r[\alpha COO^{-}(His)\cdots\xi C(Arg259)]$ is such that the interaction due to the hydrogen bonding is most favorable. The interaction is gradually lost with an increase in mutual separation and is unfavorable also at the closer separation due to the short-range repulsion between ATP, His, and Arg-259. In contrast, the corresponding energy surface of the D-His is largely unfavorable due to the unfavorable electrostatic interaction of the positively charged amino group of His with the positively charged guanidinium group of Arg-259.

The energy surface as a function of relative distance between δN of His and ηH of Tyr 264 (indicated as $\Delta r[\delta N\ (His)\cdots\eta H(Tyr\ 264)]$) and the chiral center of His and ηH of Tyr-264 (indicated as $\Delta r[C^{*}(His)\cdots\eta H(Tyr\ 264)]$) for $Model_{Reactant(L)}$ as well as $Model_{Reactant(D)}$ with rigid geometry are shown in the Figures 8(a) and 8(b), at the HF/6-31G**:PM3 level of theory including Tyr 264 at the HF level and the PM3 level, respectively. The figures show that the energies of the $Model_{Reactant(L)}$ and $Model_{Reactant(D)}$ as a function of $\Delta r[\delta N\ (His)\cdots\eta H(Tyr\ 264)]$ and $\Delta r[C^{*}(His)\cdots\eta H(Tyr\ 264)]$ are more favored for the $Model_{Reactant(L)}$ relative to the $Model_{Reactant(D)}$ on average. As the relative separation between $\Delta r[\delta N\ (His)\cdots\eta H(Tyr\ 264)]$ decreases, the hydrogen bonding between His and Tyr-264 is favored, and consequently the energy surface of $Model_{Reactant(L)}$ passes through a minimum as shown in Figures 8(a) and 8(b), respectively. The results indicate that the interaction of L-His and the surrounding residues is more favorable than the interaction of the same residues with D-His. This indicates that the network of interaction (principally electrostatic) is highly unfavorable when the D-amino acid is incorporated.

The optimized geometries of the reactant, transition state, and product of the activation step using ONIOM (HF/3-21G*:PM3 level) calculation are shown in Figures 9(a−c), respectively. The comparison of the geometries confirms the in-line displacement mechanism in which the oxygen atom of the carboxylic group attacks the phosphorus atom of the α-phosphate group as proposed from crystallographic studies. The tetrahedral arrangement of the oxygen atoms (around the phosphorus atom) in the α-phosphate group inverts through a planar state in going to the product state from the reactant. This can be noted from a comparison of the bond angles and distances around the α-phosphate group in the optimized geometries of the reactant, transition state, and product. The $(His)O\cdots P-O_{(1)}(ATP)$ is changing from 73.05° (reactant) via 101.91° (transition state) to 106.80° (product). Similarly, the $(His)O\cdots P-O_{(2)}(ATP)$ is changing from 71.72° (reactant) via 96.29° (transition state) to 104.55° (product), and the $(His)O\cdots P-O_{(3)}(ATP)$ is changing from 82.05° (reactant) via 90.56° (transition state) to 100.45° (product) (we referred to the oxygen of the carboxylic of His attacking at α-P as (His)O, and three oxygens attached to the α-phosphate group are referred to as $O_{(1/2/3)}(ATP)$, respectively). While the $(His)O\cdots P(ATP)$ separation is decreasing from 3.43 Å (reactant) via 1.74 Å (transition state) to 1.66 Å (product) upon formation of the O−P bond in adenylate, the $P(ATP)\cdots O_{(4)}$ (ATP) separation is changing from 1.65 Å (reactant) via 2.70 Å (transition state) to 6.76 Å (product) as the phosphate group leaves. The scheme of the reaction is shown in Figure 10. The variation in the bond angles and distances demonstrates the attack of the carboxylic oxygen at the α-P and the concomitant inversion of oxygen atoms around α-P. The transition state structure containing D-His lacks the hydrogen bond network as present in the L-His case and is unfavorable.

The change in the electrostatic potential during the course of the reaction is shown for the reactant and the product state in Figures 11(a) and 11(b), respectively. $V(\vec{r})$ increases to a maximum at the nucleus which is noted from the nature of electrostatic potential at His and ATP. An intervening region of lower (negative) electrostatic potential is noted between His and ATP in the reactant state (Figure 11(a)) which facilitates the approach of these two moieties. The analysis of the electrostatic potential is also useful to understand the role of the Mg^{2+} ion and Arg 259 and Arg 113 residues near the reaction center. Mg^{2+} ion dependence of class I and class II synthetases is well-known, with one Mg^{2+} ion being required for class I and three for class II.[22] It is noted that the Arg 259 is specific for His synthetase, while other class II enzymes have Mg^{2+}. Arg-259 is suggested to act as a substitute for one of the three Mg^{2+} ions present[4,22] (Mg^{2+} 1 near the α and β phosphate). It is noted that the presence of the two Mg^{2+} ions located near the β−γ phosphate linkage (indicated as Mg^{2+} 2 and Mg^{2+} 3) is responsible for reducing the negative charge densities over the oxygen atoms attached to the β and γ phosphate and thereby facilitating the nucleophilic attack by the carboxylic group of His at the phosphorus of the α-phosphate group. The electrostatic potential around the α-phosphate group is negative. The electrostatic potential of the phosphate group of the ATP molecule in the presence of Mg^{2+} 2 and Mg^{2+} 3 excluding Arg 113 and Arg 259 is shown in Figure S.4(a) of the Supporting Information. The electrostatic potential of the phosphate group of the ATP and His molecule (as present in the reactant state) in the presence of the Mg^{2+} 2 and Mg^{2+} 3 excluding Arg 113 and Arg 259 is shown in Figure S.4(b) of the Supporting Information. Thus, the α-phosphate group of ATP alone is unfavorable for the in-line mechanism of nucleophilic attack by the electron density of the carboxylic group of His in the absence of the Arg residues. The electropositive potential around the phosphate groups of ATP can be noted when the Arg 113 and Arg 259 residues (as belonging to the motif 2 and His A loop) are included. This is shown in Figure S.5(a) and S.5(b) of the Supporting Information, respectively. Consequently, the Arg 259 residue has a similar role as played by the two Mg^{2+} cations, as this residue is in close proximity of the α-P of ATP. Arg 113 also facilitates the reduction of negative charge on the other side of the reaction center.

The favorable electrostatic interaction of Arg 113 and Arg 259 with ATP and His is also shown from the calculation of binding energy of Arg 259 when the charges over the guadinium side chain of Arg 259 are reduced by replacement of the $-NH_2$ groups with methyl groups. The extrapolated binding energy of the Arg 259 is −96.23 kcal/mol in the reactant state calculated at the level of the two-level ONIOM (HF/3-21G*:PM3//HF/3-21G*:PM3) method using ONIOM level extrapolated energy. When the $-NH_2$ groups of Arg 259 are replaced by $-CH_3$ groups, the binding energy reduces to −15.58 kcal/mol. The significant loss of interaction energy is due to loss of electrostatic interaction of the Arg 259 with the reactants.

A look into the hydrogen bonding pattern of the Arg 113 and Arg 259 with His and ATP reveals a more significant role of the Arg 259 in the reaction pathway than the charge neutralization alone as shown in Figure 12. The variations of the hydrogen bonding pattern in the reactant, transition state, and product as calculated in the present work are described in section B of the Supporting Information. The variation in the

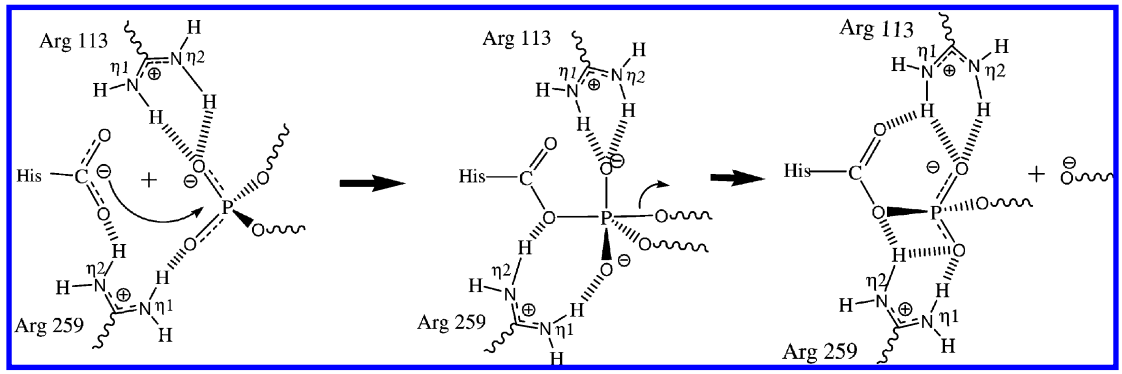

Figure 12. Schematic diagram showing hydrogen bonding interaction of the active site residues with the reacting substrates in the optimized geometries of the (a) reactant, (b) transition state, and (c) product of the activation step of aminoacylation reaction using the ONIOM (HF/3-21G*:PM3) level of calculation as shown in Figure 9. The structural parameters are shown in Table I.

TABLE I: Selected Structural Parameters Describing the Hydrogen Bonding Pattern in the Reactant, Transition State, and Product for the Activation Step of Aminoacylation Reaction in the Model of HisRS Calculated at the ONIOM (HF/3-21G*// PM3) Level of Theory (See Text for Details)[a]

active site residue hydrogen bonded with reactant moiety	reactant moiety	atom in active site residue[b]	atom in reactant[b]	distance in reactant state (Å)	distance in transition state (Å)	distance in product state (Å)
Arg-259	ATP	H atom attached with η_1 N (65)	O atom attached with α P atom of ATP (32)	1.60	1.69	1.94
Arg-259	His	H atom attached with $\eta 2$ N (63)	O atom of carboxylic acid group of His (71)	1.81	2.16	2.75
Arg-259	ATP	H atom attached with $\eta 2$ N (63)	O atom attached with α P atom of ATP (32)	2.95	2.09	1.89
Arg-113	ATP	H atom attached with $\eta 2$ N (54)	O atom attached with α P atom of ATP (36)	1.85	1.83	1.70
Arg-113	ATP	H atom attached with $\eta 1$ N (53)	O atom attached with α P atom of ATP (36)	1.98	1.91	1.98

[a] A cut-off of 3 Å is used to measure the hydrogen bond length. The distances are expressed in Å. [b] Numbering scheme is shown in Figure S.6 of the Supporting Information.

pattern indicates that while the Arg 113 maintains contact principally with the α-phosphate group the Arg 259 anchors the His as well as the α-phosphate group from the reactant state to the transition state. The hydrogen bonding pattern of Arg 259 with the adenylate is similar to those present in the reactant and the transition state. The hydrogen bond lengths measured within a cutoff distance of 3 Å between Arg residues (Arg 259 and Arg 113) and reactants (His or ATP), respectively, are shown in Table I. While the Arg 259 retains hydrogen bonding with His and ATP in reactant and product via transition state, the Arg 113 is hydrogen bonded only with ATP. The change in the hydrogen bonding pattern from the reactant to product via transition state demonstrates that the Arg 259 anchors the carboxylic acid group of His and the oxygen atom of the α-phosphate group in the reaction pathway. This residue is in closer proximity with the reactants than that with the Arg 113. The latter residue principally retains proximity with one oxygen atom of the α-phosphate group throughout the course of the reaction. Consequently, the Arg 259 plays a more important catalytic role in the activation step rather than merely reducing the negative charge density over the ATP. This catalytic act by Arg 259 is essentially dependent on hydrogen bonding. Such catalytic activity with the aid of hydrogen bonding is noted in other biologically important reactions like peptide bond formation.[6]

To confirm the catalytic role of the Arg 259, we computed the transition state barrier height of the reaction by altering the capacity of the residue to form hydrogen bonds. The NH_2 groups of the side chains of Arg 259 are replaced by CH_3 groups. The corresponding reactant, transition state, and product geometries are shown in the Figures 13(a−c), respectively. The barrier height with modified residue is rather high compared to the case when Arg 259 is present (Figure 14). This result conclusively proves that Arg 259 has a catalytic role by anchoring the His and ATP via hydrogen bonding.

The present study reveals multiple factors that control the fidelity of the activation step of aminoacylation reaction and control the precision and retention of the biological homochirality. The surrounding amino acids in the active site of HisRS are located within a nanoscale distance. These residues, through a network of electrostatic interactions, impose stringent chiral discrimination in the aminoacylation reaction. Other than the factors such as the chiralities of the substrates, surrounding amino acids in active site, their confinement, and proximity in the cavity in a nanoscale range, the influence of the network of electrostatic interactions present in the active site has a significant role in fidelity mechanisms. Further studies in other class I and class II synthetases might reveal the intricate nature of the electrostatic interaction present in each specific case.

A variety of complex biological and biomimetic systems have microheterogeneity. The environment of the nanospace of the active site as investigated here is one of them. Detailed studies revealed that enhanced molecular interaction and multisite interaction are also features of the recognition phenomena at the microscopically heterogeneous interfaces.[25−27] The discrimination exhibited by the synthetase is essentially controlled by the preferential interactions at multiple sites. It is worthwhile to explore the unifying principles underlying the preferential interaction and discrimination as exhibited by various complex systems in general. Further studies in this direction are ongoing.

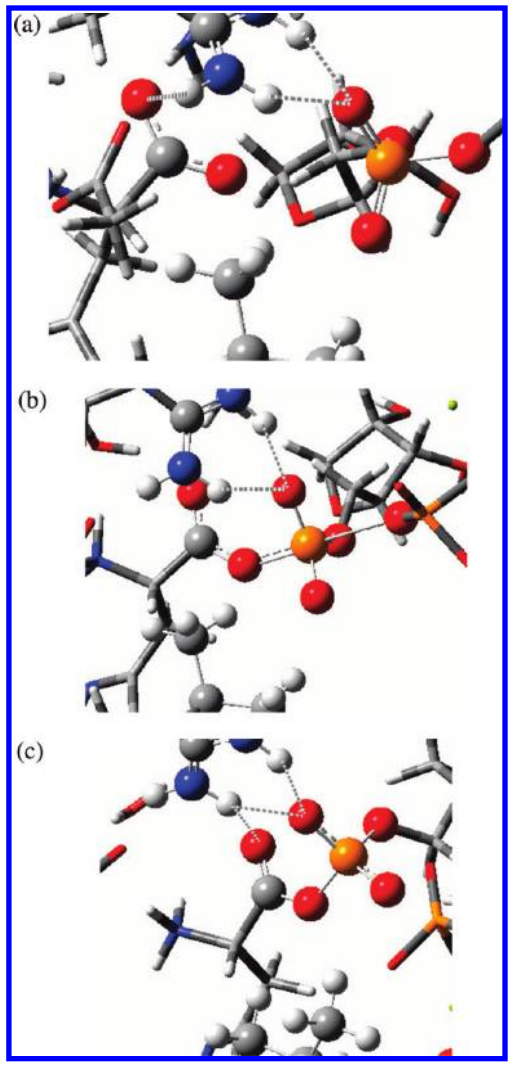

Figure 13. Optimized geometries of the (a) reactant, (b) transition state, and (c) product of the activation step of the aminoacylation reaction with modified Arg-259 (the $-NH_2$ groups of the guadinium side chains of the Arg 259 residue are replaced by the $-CH_3$ group; details in the theoretical section) using the ONIOM (HF/3-21G*:PM3) level of theory. The Cartesian coordinates are given in the Table II(e) of the Supporting Information.

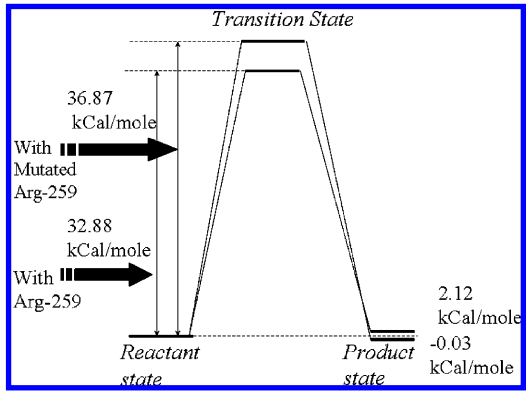

Figure 14. Comparison of the transition state energy level diagram of the activation step of the aminoacylation reaction with Arg-259 and modified Arg-259. The details are given in the theoretical section. The relative energies (with respect to the reactant) are expressed in kcal/mol.

IV. Conclusions

Summarizing, we carried out a combined ONIOM (*ab initio*/semiempirical) calculation for the activation step of aminoacylation reaction in histidyl-tRNA synthetase (HisRS). The study of the variation in the energy during the mutual approach of the His and ATP to form adenylate shows that the surrounding nanospace of the synthetase confines the L-His and ATP to proximally place the reactants in geometry suitable for the in-line nucleophilic attack. The significantly higher energy of the model containing D-His is due to unfavorable interaction of D-His with ATP and surrounding residues. The confinement of reacting moieties placed within the nanometer regime of an active site drives the corresponding reaction very precisely with remarkable discrimination capacity. Interaction of L-His and the surrounding residues is more favorable than the interaction of the same residues with D-His. This indicates that the network of interaction (principally electrostatic) is highly unfavorable when the D-amino acid is incorporated. The reorganization of the surrounding nanospace can lower the unfavorable nature of the interaction energy surface of D-His and surrounding residues. However, such a rearrangement requires large-scale structural reorganization of the synthetase structure which is disruptive for overall structure of the synthetase. The variation in the bond angles and distances in the reactant and transition state demonstrates the attack of the caroboxylic oxygen at the α-P which is accompanied by a decrease in the corresponding separation and bond formation as well as an increase in the separation between the oxygen (attached between α-P and β-P) and α-P which leaves as PP_i. The concomitant inversion of oxygen atoms around α-P is also observed. Calculation of the electrostatic potential indicates that in addition to the Mg^{2+} the Arg residues in the active site facilitate the nucleophilic attack by reducing the negative charge distributed over the oxygen atoms attached to the α-P of ATP. The Arg 259 residue has a similar role as played by the two Mg^{2+} cations, as this residue is in close proximity of the α-P of ATP. Arg 113 also facilitates the reduction of negative charge on the other side of the reaction center. The favorable electrostatic interaction of the Arg 259 with ATP and His is also supported from the calculation of binding energy. The change in the hydrogen bonding pattern from the reactant to the product via a transition state demonstrates that the Arg 259 anchors the carboxylic acid group of His and the oxygen atom of the α-phosphate group in the reaction pathway. To the best of our knowledge, the present work is the first calculation of the transition state of the activation step. The study shows that Arg 259 plays an important catalytic role in the activation step rather than merely reducing the negative charge density over the ATP. The hydrogen bonding interaction is lost when the NH_2 groups of the side chains of Arg 259 are replaced by CH_3 groups. The transition state barrier height is unfavorable in the latter case which further confirms the catalytic act by Arg 259.

Acknowledgment. This work is supported by a grant from DST, India. S.D.B. thanks the University of Kalyani for a research scholarship. A part of the calculation was carried out at B.I.T.S. Pilani.

Supporting Information Available: Additional tables, figures, and experimental data. This material is available free of charge via the Internet at http://pubs.acs.org.

References and Notes

(1) Nelson, D. L.; Cox, M. M. *Lehninger Principles of Biochemistry*, 4th ed.; W. H. Freeman & Co.: New York, 2002; p 1044.
(2) Ibba, M.; Söll, D. *Annu. Rev. Biochem.* **2000**, *69*, 617.
(3) Berg, J. M.; Tymoczko, J. L.; Stryer, S. *Biochemistry*; W. H. Freeman & Co.: New York, 2002; p 671.

(4) Arnez, J.; Harris, G.; Mitschler, D. C.; Rees, B.; Francklyn, C. S.; Moras, D. *EMBO J.* **1995**, *14*, 4143.
(5) Åberg, A.; Yaremchuk, A.; Tukalo, M.; Rasmussen, B.; Cusack, S. *Biochemistry* **1997**, *36*, 3084.
(6) Nandi, N. *Int. Rev. Phys. Chem.* **2009**, *28*, 111.
(7) Davie, E. W.; Konigsberger, V. V.; Lipman, F. *Arch. Biochem. Biophys.* **1956**, *65*, 21.
(8) Calendar, R.; Berg, P. *Biochemistry* **1966**, *5*, 1690.
(9) Soutourina, J.; Plateau, P.; Blanquet, S. *J. Biol. Chem.* **2000**, *275*, 32535.
(10) Bergmann, F.; Berg, P.; Dieckmann, M. *J. Biol. Chem.* **1961**, *236*, 1735.
(11) Norton, S.; Ravel, J.; Lee, C.; Shive, W. *J. Biol. Chem.* **1963**, *238*, 269.
(12) Yamane, T.; Miller, L.; Hopfield, J. J. *Proc. Natl. Acad. Sci. U.S.A.* **1974**, *71*, 4135.
(13) Tamura, K.; Schimmel, P. *Science* **2004**, *305*, 1253.
(14) Thompson, D.; Lazennec, C.; Plateau, P.; Simonson, T. *J. Biol. Chem.* **2007**, *282*, 30856.
(15) (a) Dutta Banik, S.; Nandi, N. *Colloid Surf. B* **2009**, *74*, 468. (b) Arnez, J. G.; Flanagan, K.; Moras, D.; Simonson, T. *Proteins: Struct., Funct. and Genet.* **1998**, *32*, 362.
(16) Archontis, G.; Simonson, T.; Moras, D.; Karplus, M. *J. Mol. Biol.* **1998**, *275*, 823.
(17) Wales, D. J.; Miller, M. A.; Walsh, T. R. *Nature* **1998**, *394*, 758.
(18) Becker, O. M.; Karplus, M. *J. Chem. Phys.* **1997**, *106*, 1495.
(19) Leach, A. R. *Molecular Modelling: Principles and Applications*, 2nd ed.; Pearson, Prentice Hall, 2001; p 279.
(20) Lim, C.; Karplus, M. *J. Am. Chem. Soc.* **1990**, *112*, 5872.
(21) Arnez, J. G.; Augstine, J. G.; Moras, D.; Francklyn, C. S. *Proc. Natl. Acad. Sci. U.S.A.* **1997**, *94*, 7144.
(22) Colominus, C.; Seignovert, L.; Härtlein, M.; Grotli, M.; Cusack, S.; Leberman, R. *EMBO J.* **1998**, *17*, 2947.
(23) Sjoberg, P.; Politzer, P. *J. Phys. Chem.* **1990**, *94*, 3959.
(24) Frisch, M. J.; Trucks, G. W.; Schlegel, H. B.; Scuseria, G. E.; Robb, M. A.; Cheeseman, J. R.; Montgomery, J. A., Jr.; Vreven, T.; Kudin, K. N.; Burant, J. C.; Millam, J. M.; Iyengar, S. S.; Tomasi, J.; Barone, V.; Mennucci, B.; Cossi, M.; Scalmani, G.; Rega, N.; Petersson, G. A.; Nakatsuji, H.; Hada, M.; Ehara, M.; Toyota, K.; Fukuda, R.; Hasegawa, J.; Ishida, M.; Nakajima, T.; Honda, Y.; Kitao, O.; Nakai, H.; Klene, M.; Li, X.; Knox, J. E.; Hratchian, H. P.; Cross, J. B.; Bakken, V.; Adamo, C.; Jaramillo, J.; Gomperts, R.; Stratmann, R. E.; Yazyev, O.; Austin, A. J.; Cammi, R.; Pomelli, C.; Ochterski, J. W.; Ayala, P. Y.; Morokuma, K.; Voth, G. A.; Salvador, P.; Dannenberg, J. J.; Zakrzewski, V. G.; Dapprich, S.; Daniels, A. D.; Strain, M. C.; Farkas, O.; Malick, D. K.; Rabuck, A. D.; Raghavachari, K.; Foresman, J. B.; Ortiz, J. V.; Cui, Q.; Baboul, A. G.; Clifford, S.; Cioslowski, J.; Stefanov, B. B.; Liu, G.; Liashenko, A.; Piskorz, P.; Komaromi, I.; Martin, R. L.; Fox, D. J.; Keith, T.; Al-Laham, M. A.; Peng, C. Y.; Nanayakkara, A.; Challacombe, M.; Gill, P. M. W.; Johnson, B.; Chen, W.; Wong, M. W.; Gonzalez, C.; Pople, J. A. *Gaussian 03*, revision C.02; Gaussian, Inc.: Wallingford, CT, 2004.
(25) Kunitake, T. *Thin Solid Films* **1996**, *284*, 9–285.
(26) Sakurai, M.; Tamagawa, H.; Inous, Y.; Ariga, K.; Kunitake, T. *J. Phys. Chem. B* **1997**, *101*, 4810.
(27) Sakurai, M.; Tamagawa, H.; Inous, Y.; Ariga, K.; Kunitake, T. *J. Phys. Chem. B* **1997**, *101*, 4817.
(28) Humphrey, W.; Dalke, A.; Schulten, K. VMD: Visual Molecular Dynamics. *J. Mol. Graphics* **1996**, *14*, 33.

JP910730S